Supporting Information for

Predictive energetic tuning of quinoid O-nucleophiles for the electrochemical capture of carbon dioxide

Abdulaziz W. Alherz,[‡⁑1] Haley A. Petersen,[†1] Nicholas R. Singstock[‡], Sohan N. Sur,[†]

Charles B. Musgrave,[⁂*‡] Oana R. Luca[†]*

[†]*Department of Chemistry and Renewable and Sustainable Energy Institute, 215 UCB, University of Colorado Boulder, Boulder CO, 80309 USA*

[⁑] *Department of Chemical Engineering, College of Engineering and Petroleum, Kuwait University, P.O. Box 5969, Safat 13060, Kuwait*

[‡]*Department of Chemical and Biological Engineering, University of Colorado, Boulder, CO 80309, United States*

[⁂]*Materials Science and Engineering Program, University of Colorado, Boulder, CO 80309, United States*

[1] These authors contributed equally.

*E-mail: oana.luca@colorado.edu and charles.musgrave@colorado.edu

1. Experimental Determination of K and ΔG

Experimental Methods

All chemicals were used as received from commercial sources except where otherwise noted. Acetonitrile (MeCN) was distilled freshly the day of use onto molecular sieves. Tetrabutylammonium hexafluorophosphate (NBu_4PF_6) was recrystallized from minimal hot methanol, collected by filtration, and dried under high vacuum overnight prior to use as supporting electrolyte. 1,4-naphthoquinone and 1,4-benzoquinone were purified by sublimation prior to use. Gas mixtures containing 5% and 30% CO_2 (balance N_2) were obtained as special order gases from AirGas.

Electrochemical data was collected on a BioLogic SP-150 Potentiostat. Cyclic voltammetry (CV) data were collected in 0.1 M NBu_4PF_6 as supporting electrolyte in MeCN and approximately 1 mM quinone analyte. A 3 mm BASI MS-2012 glassy carbon working electrode was used with a single-junction silver wire pseudoreference, referenced externally to the ferrocene/ferrocenium (Fc/Fc^+) couple in acetonitrile, with a platinum wire counter electrode. External referencing to Fc/Fc^+ took place at the beginning, middle, and end of the set of experiments for each quinone to verify minimal drift of reference potential over time. Uncompensated resistance was assumed to have minimal effect on the electrochemical measurements due to the use of high concentration supporting electrolyte and small cell geometry with minimal interelectrode distance. Additionally, all quantitative results derived from CVs were obtained by taking the difference between two measured potentials from the same solution, effectively cancelling out the approximately constant uncompensated resistance before use in subsequent analyses. Before CVs were taken, the solution was sparged thoroughly with the gas of interest through an MeCN bubbler vial to minimize solvent evaporation. CVs were then taken under Ar, 5% CO_2, 30% CO_2, and 100% CO_2, and the change in the second reduction potential under each CO_2 gas was compared to that under Ar. The local uncorrected barometric pressure at the time of data collection was obtained from the National Center for Atmospheric Research Foothills Lab.[1]

Derivation and Analysis

The main manuscript contains a detailed description of the derivation of the equations used herein for the electrochemical determination of the free energy of CO_2 binding for each quinone.

CO_2 concentrations corresponding to the three CV conditions were found using a Henry's Law calculation. The local uncorrected barometric pressure for the time of data collection was first obtained.[1] The literature vapor pressure of acetonitrile[2] in the headspace of the vial at room temperature was then subtracted from this value to obtain a net headspace pressure. The partial pressure of CO_2 in the headspace was then obtained by multiplying this net headspace pressure by the fraction of CO_2 of the gas used to sparge the solution (5%, 30%, or 100% CO_2). This partial pressure was corrected by a fugacity correction factor of 0.995 in accordance with the methods of Gennaro et al., and the Henry's constant for CO_2 in acetonitrile at 25 °C was used to determine the mole fraction and subsequently the molar concentration of CO_2 in solution.[3]

Error for the experimental ΔG_{bind} was propagated using a standard partial derivative model with the uncertainty in K as obtained from the Origin 2019b fit.

2. Electrochemical Data

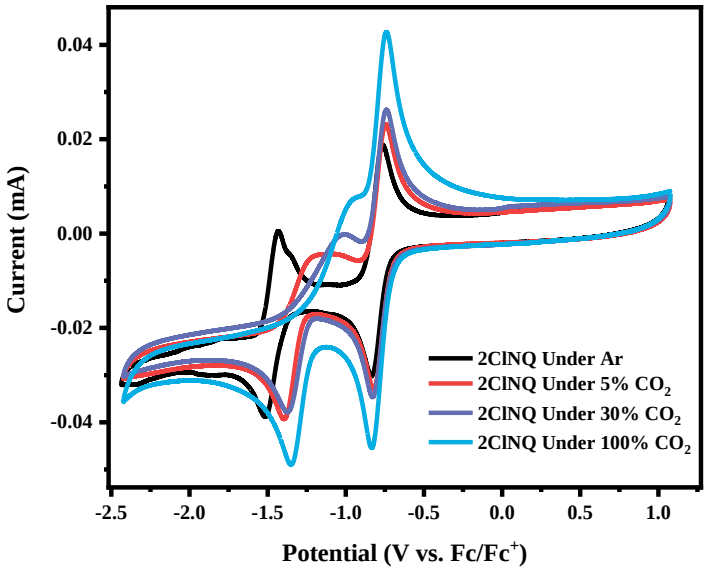

Figure S2.1. Cyclic voltammograms of 1 mM solutions of 2ClNQ in MeCN with NBu_4PF_6 in Ar with scan rate 50 mV/s and under 5% CO_2, 30% CO_2 and 100% CO_2. Working electrode: Glassy carbon; Counter electrode: Pt wire; Reference electrode: Single-junction Ag electrode referenced externally vs. Fc/Fc^+.

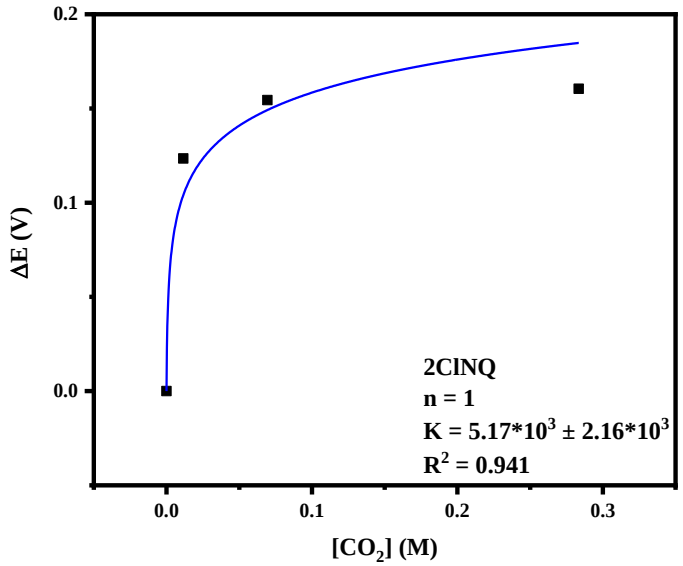

Figure S2.2. 2ClNQ: Plot of ΔE as a function of [CO_2] from data in Fig S2.1 fitted to $\Delta E_{\frac{1}{2}} = \frac{RT}{F}\ln(K[CO_2]^n + 1)$ with n = 1.

For 2ClQ, which exhibited a favorable free energy of binding for the first equivalent of CO_2 but a DFT-calculated free energy of binding of +0.9 kcal/mol for the second equivalent of CO_2, we investigated both possible binding stoichiometries. As shown below, the only mildly uphill second CO_2 binding event is not enough to preclude binding of a second CO_2 under experimental conditions, and n = 2 was demonstrated to be the better descriptor of binding.

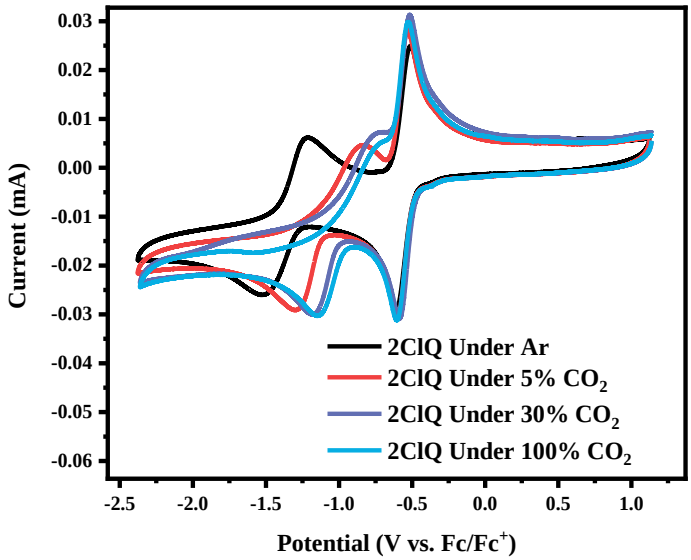

Figure S2.3. Cyclic voltammograms of 1 mM solutions of 2ClQ in MeCN with NBu_4PF_6 in Ar at 50 mV/s and under 5% CO_2, 30% CO_2, and 100% CO_2. Working electrode: Glassy carbon; Counter electrode: Pt wire; Reference electrode: Single-junction Ag electrode referenced externally vs. Fc/Fc^+.

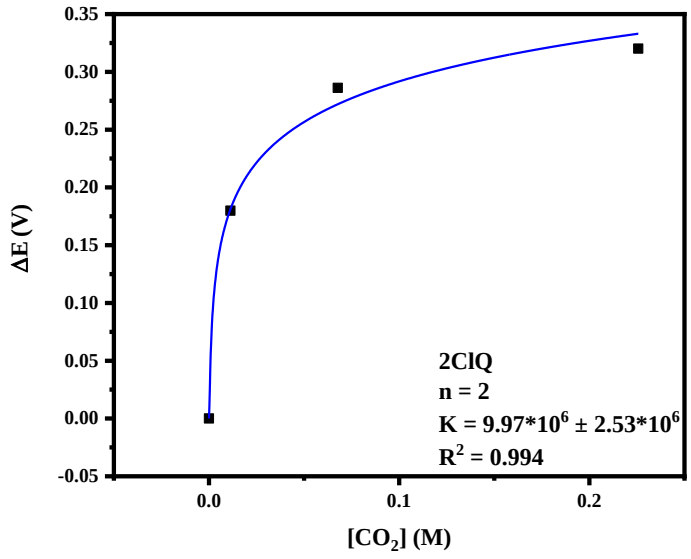

Figure S2.4. 2ClQ: Plot of ΔE as a function of $[CO_2]$ from data in Fig S2.3, fitted to $\Delta E_{\frac{1}{2}} = \frac{RT}{F}\ln(K[CO_2]^n + 1)$ with n = 2.

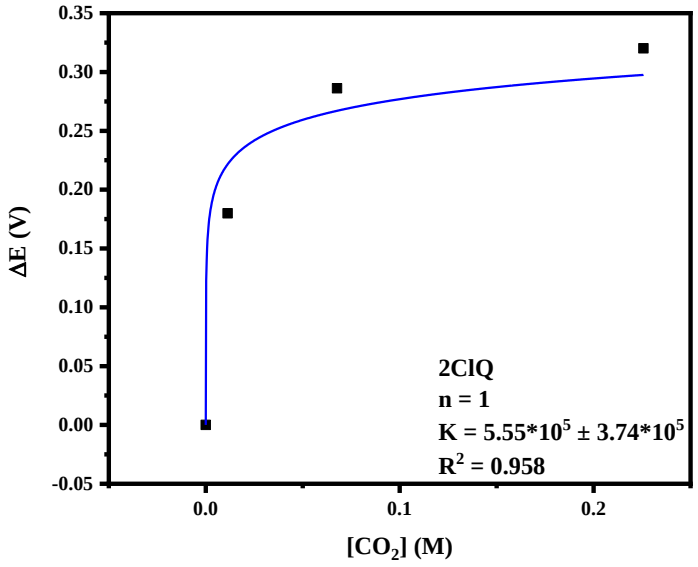

Figure S2.5. 2ClQ: Plot for 2ClQ of ΔE as a function of [CO_2] used in each CV experiment from Figure S2.3, fitted to $\Delta E_{\frac{1}{2}} = \frac{RT}{F}\ln(K[CO_2]^n + 1)$ with n = 1. The lower R^2 of this fit, as compared to that with n = 2, is indicative that the binding of 2ClQ is better described by 2:1 stoichiometry of CO_2 to quinone.

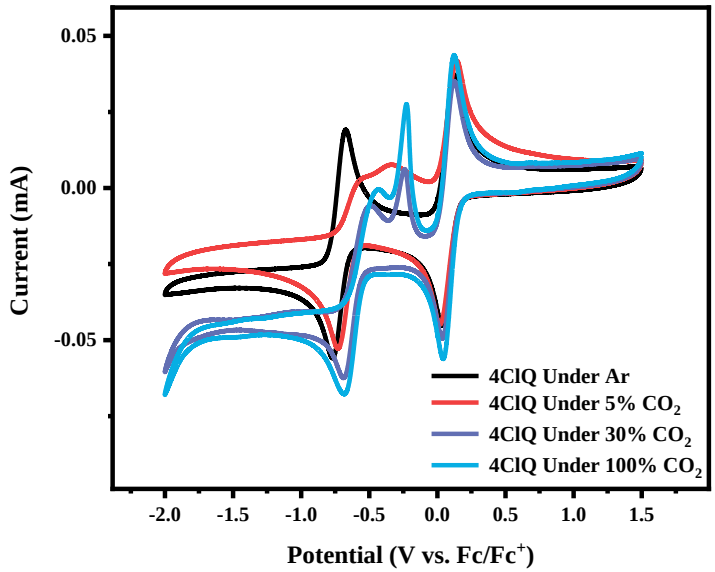

Figure S2.6. Cyclic voltammograms of 1 mM solutions of 4ClQ in MeCN with NBu_4PF_6 in Ar at 50 mV/s and under 5% CO_2, 30% CO_2, and 100% CO_2. Working electrode: Glassy carbon; Counter electrode: Pt wire; Reference electrode: Single-junction Ag electrode referenced externally vs. Fc/Fc^+. The appearance of an additional oxidation feature in the presence of increasing concentrations of CO_2 is attributed to the oxidation of the dianionic CO_2 adduct $4ClQ(CO_2)^{2-}$.[4]

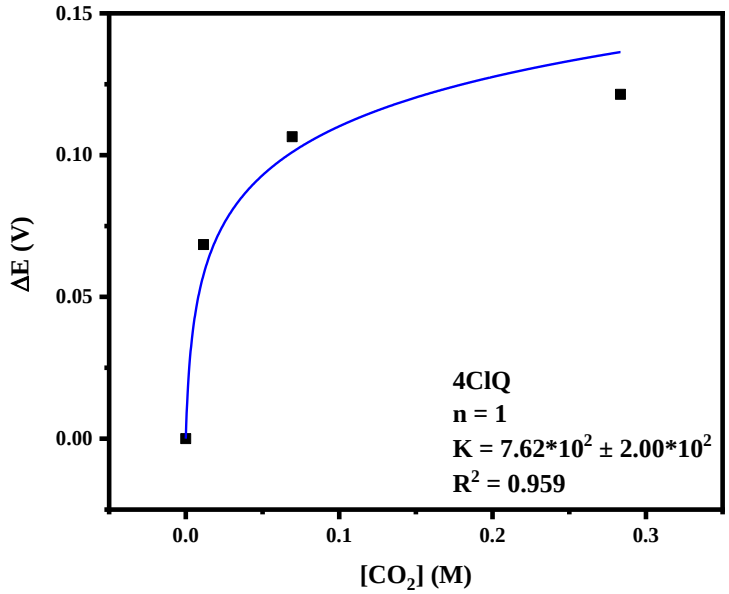

Figure S2.7. Plot for 4ClQ of ΔE as a function of [CO_2] used in each CV experiment from Figure S2.6, fitted to $\Delta E_{\frac{1}{2}} = \frac{RT}{F}\ln(K[CO_2]^n + 1)$ with n = 1.

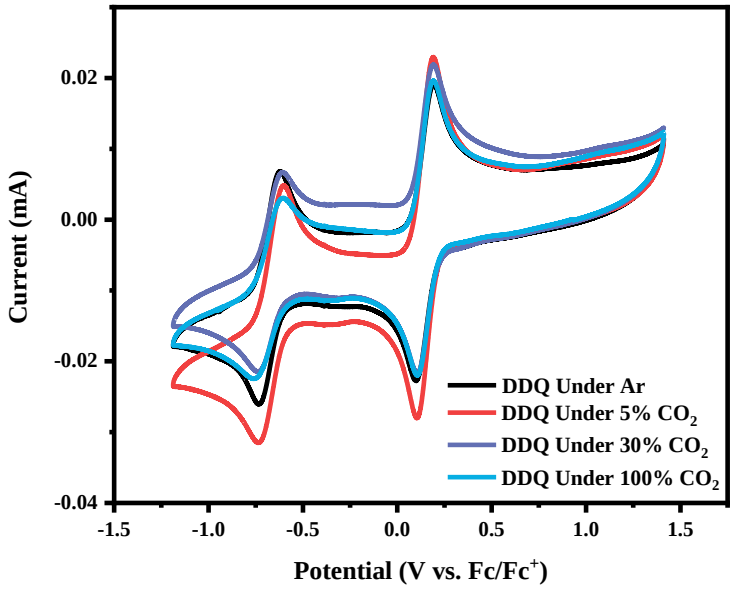

Figure S2.8. Cyclic voltammograms of 1 mM solutions of DDQ in MeCN with NBu_4PF_6 in Ar with scan rate 50 mV/s and under 5% CO_2, 30% CO_2, and 100% CO_2. Working electrode: Glassy carbon; Counter electrode: Pt wire; Reference electrode: Single-junction Ag electrode referenced externally vs. Fc/Fc^+. The lack of shift in the potential of the second reduction feature illustrates that there is negligible CO_2 binding to DDQ.

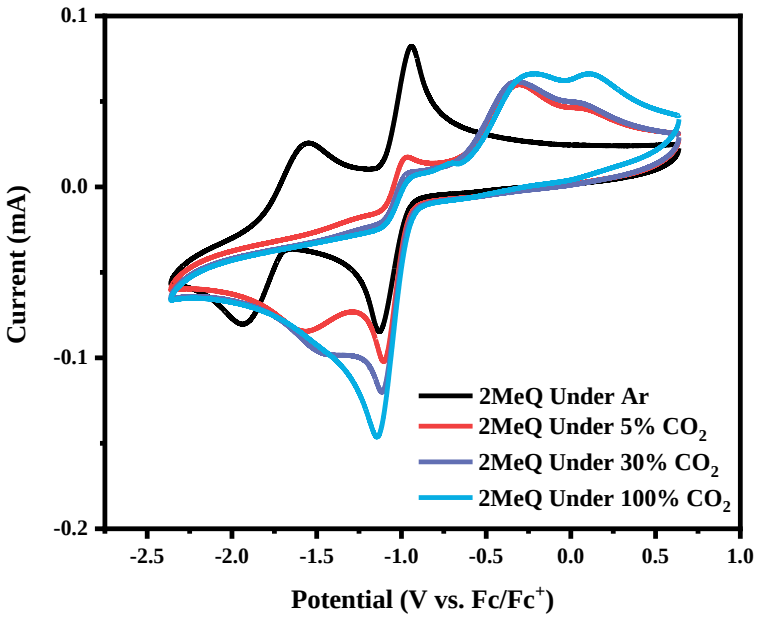

Figure S2.9. Cyclic voltammograms of 1 mM solutions of 2MeQ in MeCN with NBu_4PF_6 in Ar at 300 mV/s and under 5% CO_2, 30% CO_2, and 100% CO_2. Working electrode: Glassy carbon; Counter electrode: Pt wire; Reference electrode: Single-junction Ag electrode referenced externally vs. Fc/Fc^+. A faster scan rate was necessary in order to observe peak separation.

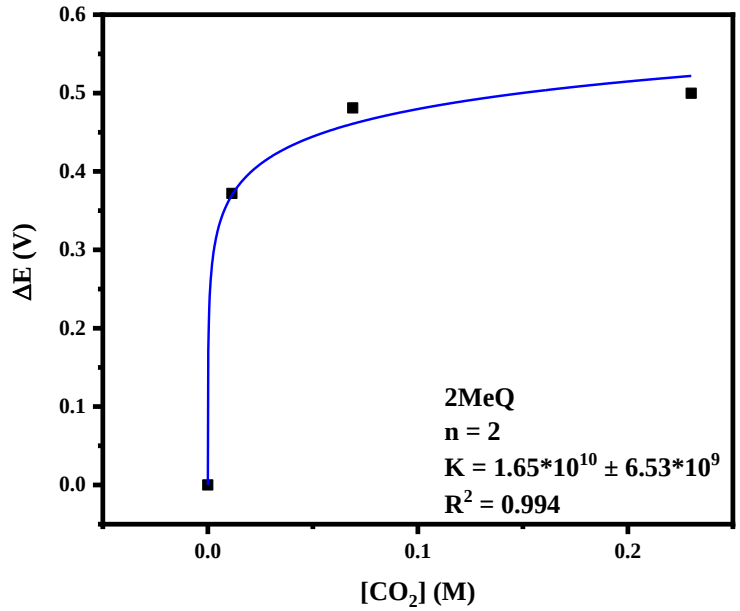

.

Figure S2.10. 2MeQ: Plot of ΔE as a function of $[CO_2]$ used in each CV experiment in Figure S2.9, fitted to $\Delta E_{\frac{1}{2}} = \frac{RT}{F}\ln(K[CO_2]^n + 1)$ with $n = 2$.

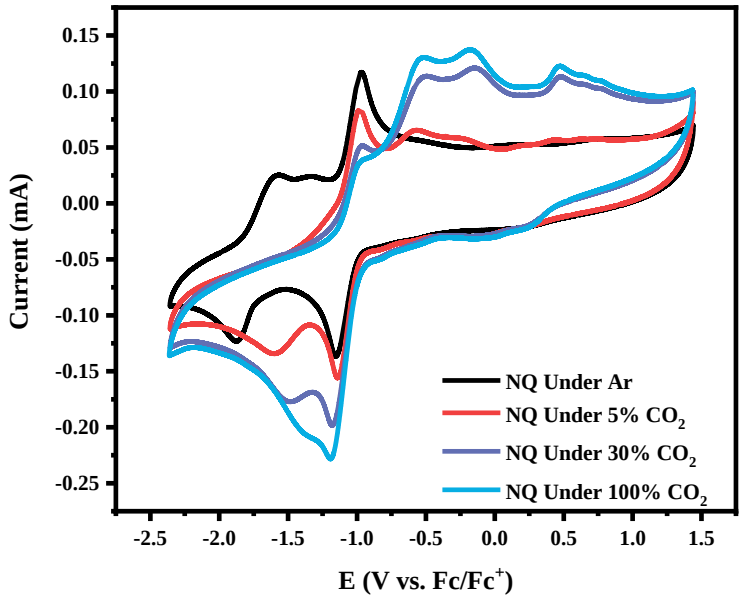

Figure S2.11. Cyclic voltammograms of 1 mM solutions of NQ in MeCN with NBu_4PF_6 in Ar at 1000 mV/s and under 5% CO_2, 30% CO_2, and 100% CO_2. Working electrode: Glassy carbon; Counter electrode: Pt wire; Reference electrode: Single-junction Ag electrode referenced externally vs. Fc/Fc^+.

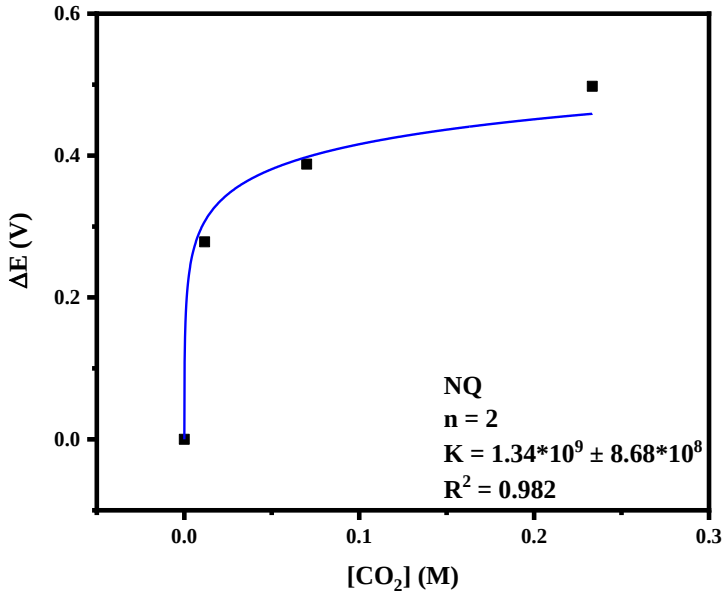

Figure S2.12. NQ: Plot of ΔE as a function of $[CO_2]$ used in each CV experiment in Figure S2.11, fitted to $\Delta E_{\frac{1}{2}} = \frac{RT}{F}\ln(K[CO_2]^n + 1)$ with $n = 2$.

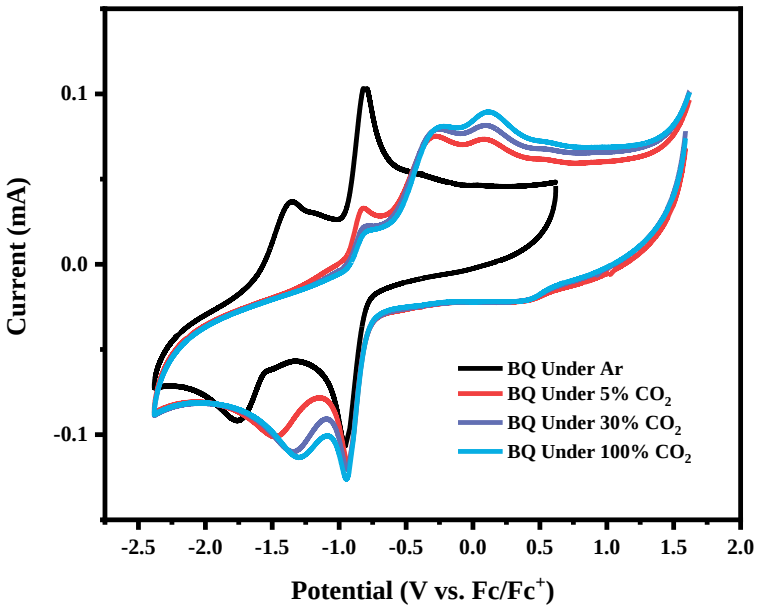

Figure S2.13. Cyclic voltammograms of 1 mM solutions of BQ in MeCN with NBu_4PF_6 in Ar at 1000 mV/s and under 5% CO_2, 30% CO_2, and 100% CO_2. Working electrode: Glassy Carbon; Counter electrode: Pt wire; Reference electrode: Single-junction Ag electrode referenced externally vs. Fc/Fc^+.

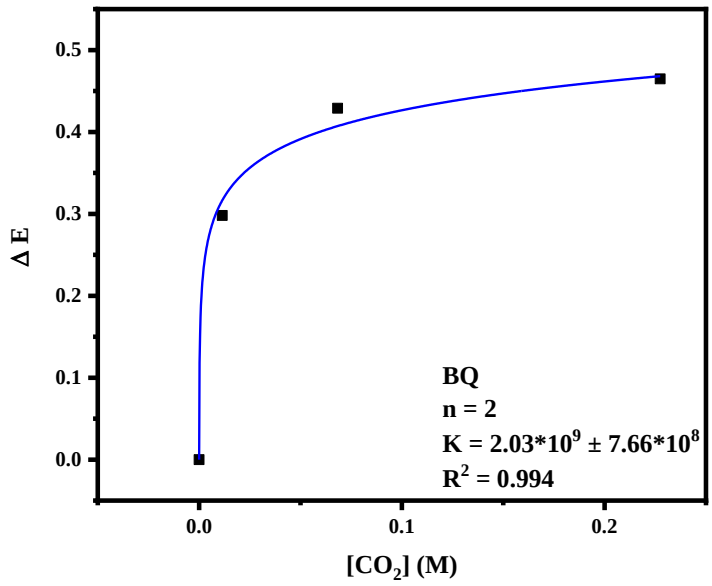

Figure S2.14. Plot for BQ of ΔE as a function of $[CO_2]$ used in each CV experiment from data in S2.13, fitted to $\Delta E_{\frac{1}{2}} = \frac{RT}{F}\ln(K[CO_2]^n + 1)$ with n = 2.

3. Computational methods

General

Density Functional Theory (DFT) calculations based on the Minnesota 15 (MN15) functional with the 6-311+G(d,p) Pople triple-zeta basis set with diffuse and polarization functions were performed in Gaussian 16 to compute optimized minimum energy geometries of quinones, their reduced and CO_2-bound intermediates and products.[5-7] The triple-zeta basis set is sufficiently large to accurately model the quinoid structures. Additionally, polarization and diffuse functions are necessary to model the anionic nature of the reduced intermediates. Reactants and products are assumed to be at infinite separation for the calculation of thermodynamic and kinetic quantities. Vibrational calculations were performed to a) confirm that there are no imaginary frequencies for reactants and products, b) compute thermal and entropic corrections, and c) verify that only one imaginary mode corresponding to the reaction coordinate exists for transition states. The SMD implicit solvent model was chosen as it is specifically optimized for Minnesota functionals to account for interactions between the solvent and sorbent molecules. [8] This method was used previously in our publication on imidazolium-based CO_2 sorbents and exhibited good agreement between experiment and theory.[9] Furthermore, MN15 has been fit to a large dataset and performs exceptionally well on organic as well as metallic systems when compared to other functionals over multiple databases.[5] This method has a Mean Absolute Deviation (MAD) of 4.6 kcal/mol for binding energies compared to experiment. As a benchmark, binding energies obtained via MN15 are compared to the wB97xD/6-311+G(d,p)/CPCM method, which performs slightly worse than MN15 with a MAD of 5.4 kcal/mol. We note that both MN15 and wB97xD functionals include dispersion corrections to accurately model organic systems. The results are shown in Tables S3.1 and S3.2. While the MAD is larger than the expected DFT error (~3 kcal/mol), it is not uncommon to encounter outliers especially with atypical systems such as dianionic quinoids. Furthermore, the agreement between the two functionals, which are derived from very different approaches, suggests that the DFT-predicted binding energies are accurate.

Reduction Potentials

Reduction potentials versus the ferrocenium/ferrocene electrode were computed using the following equation:

(13) $$E_{red} = V(G_X - G_{X-}) - C,$$

Where V = 27.2114 V/Hartree conversion factor, C is 4.988, the absolute reduction potential of the Fc+/Fc electrode as determined by Cossi[10], and $(G_X - G_{X-})$ corresponds to the Free Energy difference between neutral and reduced species. Reduction potential values reported in the main text were computed using the wB97xD/6-311+G(d,p)/CPCM method, as it predicted values that were more accurate relative to experiment compared to the MN15 functional.[11, 12] Both methods performed exceptionally in predicting the first reduction potential E_1, with a MAD of 0.1 eV. However, the accuracy of both functionals declines for predicting the second reduction potential E_2, with the errors more pronounced for the MN15 functional (MAD = 0.47 V) compared to wB97xD (MAD = 0.37 V). While MN15 is superior in predicting thermochemical properties such as binding energies, Minnesota functionals are highly parametrized and overfit to energetic properties, such as reaction enthalpies and barriers, rendering them less predictive of other properties that are not included when training the functional, such as reduction potentials, especially for systems that are excluded from ordinary databases,[5, 13-15] such as the dianion quinoid structure generated with the second reduction. It is worth noting that the errors from experiment with both DFT methods are relatively systematic, where the reduction potentials are overestimated relative to experiment. These errors can be significantly reduced with a correction term equivalent to the MAD. Figures S3.2 and S3.3 demonstrate the linearity between experimental and DFT-predicted E_1 and E_2 values.

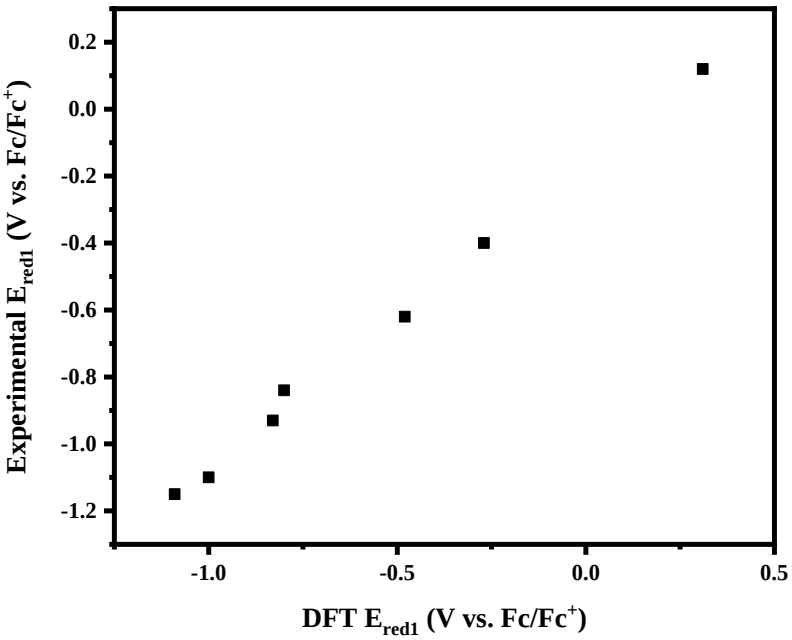

Figure S3.2. Experimental vs DFT-predicted E_1 values (V vs. Fc+/Fc). DFT data was obtained using wB97xD/6-311+G(d,p)/CPCM.

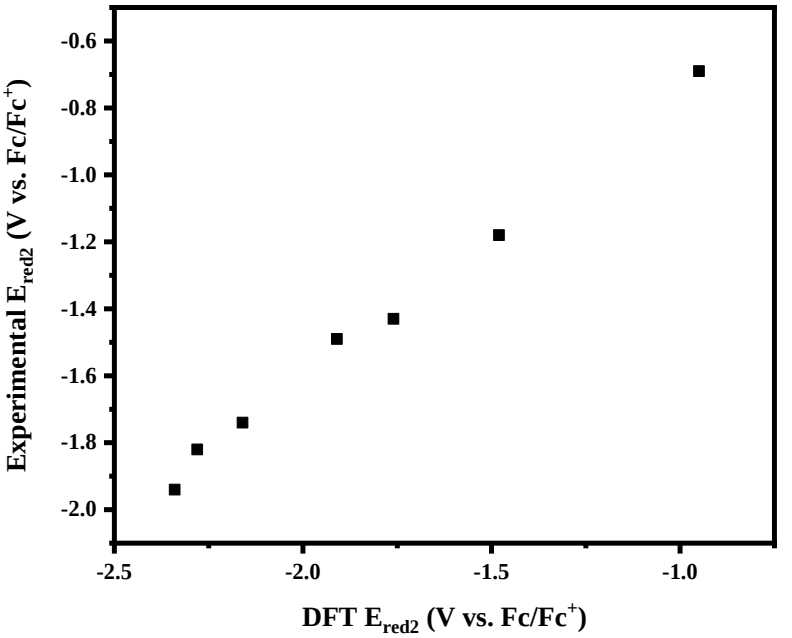

Figure S3.3. Experimental vs DFT-predicted E_2 values (V vs. Fc+/Fc). DFT data was obtained using wB97xD/6-311+G(d,p)/CPCM.

System of Chemical Equations:

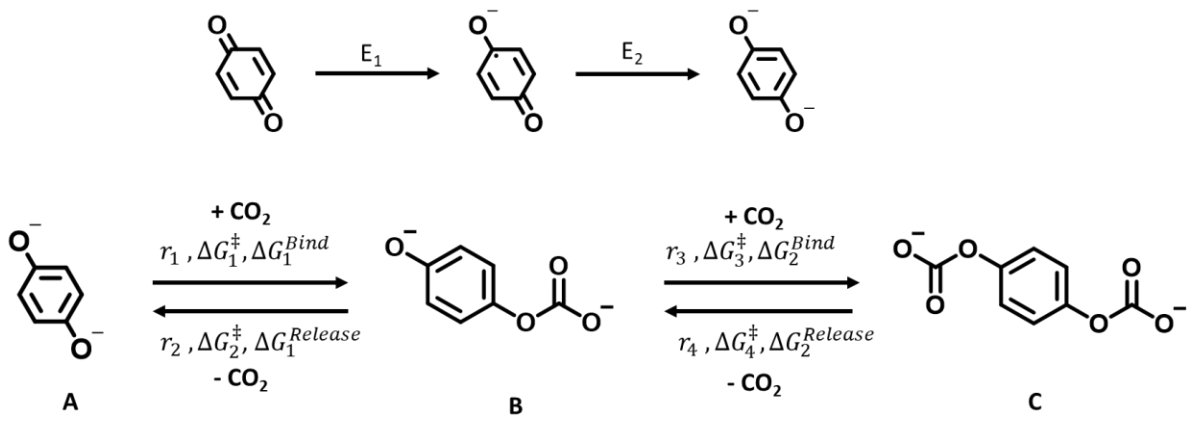

$$\Delta G_1^{\ddagger} = G_{TS1} - G_A - G_{CO2(solv)} \qquad \Delta G_3^{\ddagger} = G_{TS2} - G_B - G_{CO2(solv)}$$

$$\Delta G_2^{\ddagger} = G_{TS1} - G_B \qquad \Delta G_4^{\ddagger} = G_{TS2} - G_C$$

Table S3.1. Data collected using the methods described above and in the main text. Reduction potentials are reported in V vs. Fc/Fc^{+}. Thermodynamic CO_2 binding energies and Activation Barriers are reported in kcal/mol.

MN15/6-311+G(d,p)/SMD	E_{red} (V vs. Fc/Fc^{+})		*ΔG_Binding*			Binding $\Delta G^{\ddagger}$*_act*		Release $\Delta G^{\ddagger}$*_act*	
Molecule	E_1	E_2	1st CO_2	2nd CO_2	*ΔG_total*	1st CO_2	2nd CO_2	1st CO_2	2nd CO_2
2ClNQ	-0.97	-2.01	-8.8	1.8	-7.0	4.9	8.2	13.7	6.3
2ClQ	-0.70	-1.91	-9.8	0.9	-8.9	4.1	6.8	13.9	5.9
4ClQ	-0.43	-1.63	-4.9	4.5	-0.5	5.1	8.3	10.0	3.8
DDQ	0.12	-1.06	3.1	11.3	14.4	7.8	12.8	4.7	1.5
Me2Q	-1.24	-2.39	-16.8	-5.9	-22.8	2.4	3.2	19.3	9.1
NQ	-1.29	-2.33	-13.7	-2.9	-16.7	4.4	6.1	18.2	9.0
Q	-1.06	-2.26	-15.1	-5.8	-20.9	5.6	5.1	20.7	10.9

Table S3.2 Results obtained using an alternative functional and solvent model (wB97xd/CPCM) to show the similarities between the predictions of both methods. This approach systematically predicted less favorable thermodynamics and kinetics by approximately 2.5 kcal/mol on average.

wB97xD/6-311+G(d,p)/CPCM	E_{red} (V vs Fc/Fc^+)		ΔG_Binding			Binding $\Delta G^{\ddagger}$_act		Release $\Delta G^{\ddagger}$_act	
Molecule	E_1	E_2	1st CO_2	2nd CO_2	ΔG_total	1st CO_2	2nd CO_2	1st CO_2	2nd CO_2
2ClNQ	-0.80	-1.91	-5.4	5.5	0.1	7.5	9.8	12.9	4.3
2ClQ	-0.48	-1.76	-6.3	4.0	-2.3	6.1	9.6	12.4	5.7
4ClQ	-0.27	-1.48	-1.5	9.0	7.5	6.7	12.6	8.2	3.7
DDQ	0.31	-0.95	6.1	14.5	20.6	10.1	15.1	4.1	0.6
Me2Q	-1.00	-2.34	-15.5	-3.6	-19.1	5.7	7.5	21.2	11.1
NQ	-1.09	-2.28	-11.8	-0.3	-12.1	7.1	8.2	18.8	8.5
Q	-0.83	-2.16	-13.9	-2.1	-16.0	6.8	8.5	20.7	10.6

Rate equations for Equilibrium Concentrations

$$\frac{d[A]}{dt} = -r_1 + r_2$$

$$\frac{d[B]}{dt} = (r_1 + r_4) - (r_2 + r_3)$$

$$\frac{d[C]}{dt} = r_3 - r_4$$

$$r_1 = k_1[A][CO_2] = v \exp\left(-\frac{\Delta G_1^{\ddagger}}{k_B T}\right)[A][CO_2]$$

$$r_2 = k_2[B] = v \exp\left(-\frac{\Delta G_2^{\ddagger}}{k_B T}\right)[B]$$

$$r_3 = k_3[B][CO_2] = v \exp\left(-\frac{\Delta G_3^{\ddagger}}{k_B T}\right)[B][CO_2]$$

$$r_4 = k_4[C] = v \exp\left(-\frac{\Delta G_4^{\ddagger}}{k_B T}\right)[C]$$

$$[A] + [B] + [C] = 0.001\ M$$

Assumptions:

- Equilibrium: $t \rightarrow \infty$
- Forward reactions are bimolecular, requiring a quinone and a CO_2 molecule combining into 1 adduct species
- Reverse reactions are unimolecular, do not dependent on $CO_{2(solv)}$ concentrations
- T = 298K
- $[CO_2] = n[\mathrm{Q}]; \qquad n = 0.01,\ 1,\ 100, 300$
- $[CO_2]$ is constant

Key:

[A] = Concentration of doubly reduced quinone, Q^{2-}

[B] = Concentration of doubly reduced quinone with 1 bound CO_2, $Q(CO_2)^{2-}$

[C] = Concentration of doubly reduced quinone with 2 bound CO_2, $(Q(CO_2)_2)^{2-}$

k_j = rate constant of reaction j

$\Delta G_j^{\ddagger}$ = Activation Free Energy of reaction j

$v = \frac{k_B T}{h}$; k_B = Boltzmann constant, h = Planck's constant

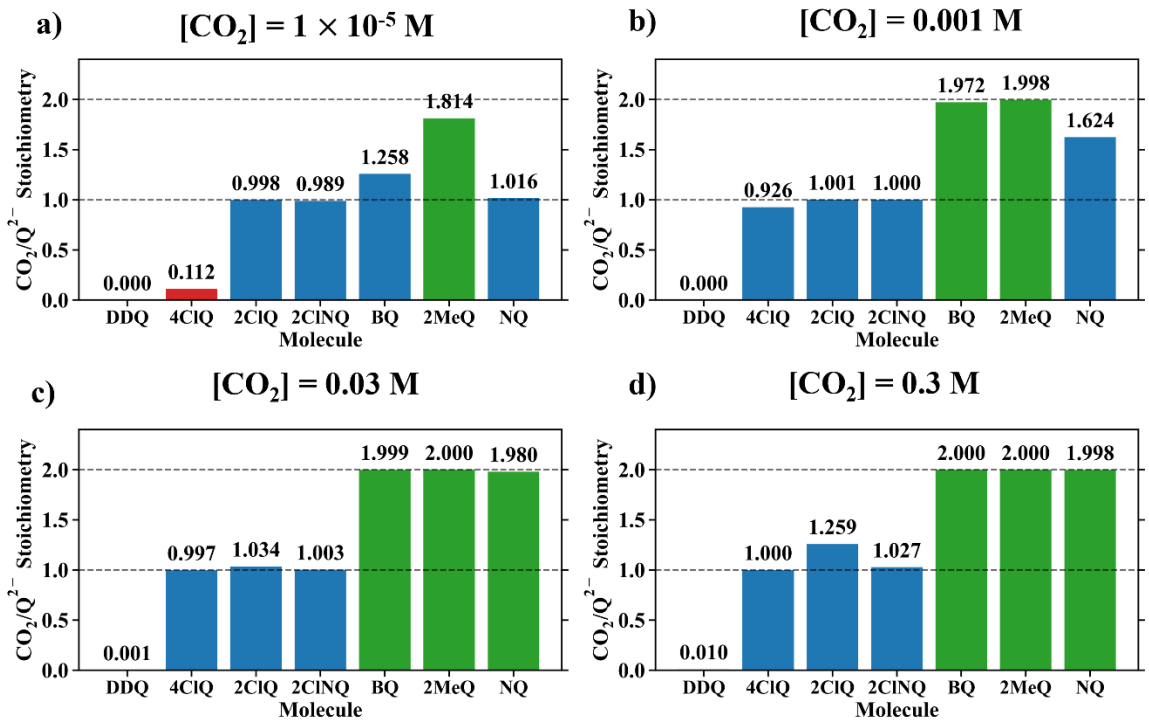

Figure S3.4. CO_2 stoichiometry relative to Q^{2-} at a) $[CO_2]$ = 1E-5 M, b) $[CO_2]$ = 0.001 M, c) $[CO_2]$ = 0.03 M, and d) $[CO_2]$ = 0.3 M, assuming the starting concentration for $[Q^{2-}]$ = 0.001 M. This model is representative of the dataset obtained using wB97xD/6-311+G(d,p)/CPCM method as opposed to what is presented in the main text.

References

1. National Center for Atmospheric Research Lab, NCAR Foothills Lab Weather. NCAR: Boulder, CO.
2. Ewing, M. B.; Ochoa, J. C. S., Vapor Pressures of Acetonitrile Determined by Comparative Ebulliometry. *Journal of Chemical & Engineering Data* **2004,** *49* (3), 486-491.
3. Gennaro, A.; Isse, A. A.; Vianello, E., Solubility and electrochemical determination of CO_2 in some dipolar aprotic solvents. *Journal of Electroanalytical Chemistry and Interfacial Electrochemistry* **1990,** *289* (1-2), 203-215.
4. Simeon, F.; Stern, M. C.; Diederichsen, K. M.; Liu, Y.; Herzog, H. J.; Hatton, T. A., Electrochemical and Molecular Assessment of Quinones as CO_2-Binding Redox Molecules for Carbon Capture. Cambridge University Press (CUP): 2021.
5. Yu, H. S.; He, X.; Li, S. L.; Truhlar, D. G., MN15: A Kohn–Sham global-hybrid exchange–correlation density functional with broad accuracy for multi-reference and single-reference systems and noncovalent interactions. *Chemical Science* **2016,** *7* (8), 5032-5051.
6. Andrae, D.; Häußermann, U.; Dolg, M.; Stoll, H.; Preuß , H., Energy-adjusted ab initio pseudopotentials for the second and third row transition elements. *Theoretica Chimica Acta* **1990,** *77* (2), 123-141.
7. Frisch, M. J.; Trucks, G. W.; Schlegel, H. B.; Scuseria, G. E.; Robb, M. A.; Cheeseman, J. R.; Scalmani, G.; Barone, V.; Petersson, G. A.; Nakatsuji, H.; Li, X.; Caricato, M.; Marenich, A. V.; Bloino, J.; Janesko, B. G.; Gomperts, R.; Mennucci, B.; Hratchian, H. P.; Ortiz, J. V.; Izmaylov, A. F.; Sonnenberg, J. L.; Williams; Ding, F.; Lipparini, F.; Egidi, F.; Goings, J.; Peng, B.; Petrone, A.; Henderson, T.; Ranasinghe, D.; Zakrzewski, V. G.; Gao, J.; Rega, N.; Zheng, G.; Liang, W.; Hada, M.; Ehara, M.; Toyota, K.; Fukuda, R.; Hasegawa, J.; Ishida, M.; Nakajima, T.; Honda, Y.; Kitao, O.; Nakai, H.; Vreven, T.; Throssell, K.; Montgomery Jr., J. A.; Peralta, J. E.; Ogliaro, F.; Bearpark, M. J.; Heyd, J. J.; Brothers, E. N.; Kudin, K. N.; Staroverov, V. N.; Keith, T. A.; Kobayashi, R.; Normand, J.; Raghavachari, K.; Rendell, A. P.; Burant, J. C.; Iyengar, S. S.; Tomasi, J.; Cossi, M.; Millam, J. M.; Klene, M.; Adamo, C.; Cammi, R.; Ochterski, J. W.; Martin, R. L.; Morokuma, K.; Farkas, O.; Foresman, J. B.; Fox, D. J. *Gaussian 16 Rev. C.01*, Wallingford, CT, 2016.
8. Marenich, A.; Cramer, C.; Truhlar, D., Universal Solvation Model of the Solvent Defined by the Bulk Dielectric Constant and Atomic Surface Tensions. *J. Phys. Chem. B* **2009,** *113*, 6378.
9. Petersen, H. A.; Alherz, A. W.; Stinson, T. A.; Huntzinger, C. G.; Musgrave, C. B.; Luca, O. R., Predictive energetic tuning of C-Nucleophiles for the electrochemical capture of carbon dioxide. *iScience* **2022,** *25* (4), 103997.
10. Barone, V.; Cossi, M., Quantum calculation of molecular energies and energy gradients in solution by a conductor solvent model. *The Journal of Physical Chemistry A* **1998,** *102* (11), 1995-2001.
11. Chai, J.-D.; Head-Gordon, M., Long-range corrected hybrid density functionals with damped atom–atom dispersion corrections. *Physical Chemistry Chemical Physics* **2008,** *10* (44), 6615-6620.
12. Steinmann, C.; Blædel, K. L.; Christensen, A. S.; Jensen, J. H., Interface of the polarizable continuum model of solvation with semi-empirical methods in the GAMESS program. *PLoS One* **2013,** *8* (7), e67725.
13. Peverati, R.; Truhlar, D. G., Quest for a universal density functional: the accuracy of density functionals across a broad spectrum of databases in chemistry and physics. *Philosophical Transactions of the Royal Society A: Mathematical, Physical and Engineering Sciences* **2014,** *372* (2011), 20120476.
14. Medvedev, M. G.; Bushmarinov, I. S.; Sun, J.; Perdew, J. P.; Lyssenko, K. A., Density functional theory is straying from the path toward the exact functional. *Science* **2017,** *355* (6320), 49-52.
15. Zhao, Y.; Truhlar, D. G., The M06 suite of density functionals for main group thermochemistry, thermochemical kinetics, noncovalent interactions, excited states, and transition elements: two new functionals and systematic testing of four M06-class functionals and 12 other function. *Theoretical Chemistry Accounts* **2008,** *120* (1-3), 215-241.